Available online at www.sciencedirect.com
SCIENCE DIRECT®
PERGAMON
International Journal of Hydrogen Energy 28 (2003) 615–623
International Journal of HYDROGEN ENERGY
www.elsevier.com/locate/ijhydene

Design considerations for a hybrid amorphous silicon/photoelectrochemical multijunction cell for hydrogen production

E.L. Miller[a,*], R.E. Rocheleau[a], X.M. Deng[b]

[a] *Hawaii Natural Energy Institute, School of Ocean and Earth Science and Technology, University of Hawaii, Honolulu, HI 96822, USA*

[b] *Department of Physics and Astronomy, University of Toledo, Toledo, OH 43606-3390, USA*

Received 1 October 2001; received in revised form 2 February 2002; accepted 1 March 2002

Abstract

Triple-junction amorphous silicon (a-Si) solar cells demonstrating photovoltaic (PV) efficiencies up to 12.7% and open-circuit voltages up to 2.3 V have recently been deposited onto stainless-steel foil substrates by the University of Toledo for photoelectrochemical (PEC) tests conducted by the University of Hawaii. The fundamental design strategy for producing such high efficiency in multijunction amorphous silicon devices involves careful current matching in each of the junctions by adjustment of the absorption spectra through bandgap tailoring. Integrated electrical/optical models are frequently used to aid in the optimization procedure, as well documented in the PV literature. Typically, the top nip junction in an a-Si triple-junction cell is designed to absorb most strongly in the 350–500 nm range. In principle, this top cell could be replaced by a PEC junction with strong absorption in a similar range to form a water-splitting photoelectrode for hydrogen production. This photoelectrode could be fabricated on SS with the back surface catalyzed for the hydrogen evolution reaction, and the front surface deposited with an a-Si:nipnip/ITO/SC structure. The top layer semiconductor (SC), which forms the PEC junction with an electrolyte, must have appropriate conduction band alignment for the oxygen evolution reaction, and the junction must be strongly absorbing in the 350–500 nm region for current matching. Possible candidate SC materials include dye-sensitized titanium dioxide (TiO_2), tungsten trioxide (WO_3), and iron oxide (Fe_2O_3). This paper discusses the specific design considerations for high solar-to-hydrogen conversion efficiency in a hybrid solid-state/PEC photoelectrode, and describes the use of integrated electrical/electrochemical/optical models developed at the University of Hawaii for the analysis of such hybrid structures. Important issues include the bias-voltage and current-matching requirements in the solid-state and electrochemical junctions, as well as fundamental quantum efficiency considerations.

Keywords: Hydrogen production; Hybrid system; Amorphous Si; Photoelectrochemical system

1. Introduction

Under the sponsorship of the US Department of Energy, in recent years the Thin Films Laboratory of the Hawaii Natural Energy Institute of the University of Hawaii has been developing high-efficiency, potentially low-cost, photoelectrochemical (PEC) systems to produce hydrogen directly from water using sunlight as the energy source. The main thrust of the work has been the development of integrated multijunction photoelectrodes, comprising low-cost semiconductor, catalytic, and protective thin films deposited on low-cost substrates (such as stainless steel), for solar hydrogen production [1]. In the illustration of a generic hydrogen photoelectrode shown in Fig. 1, sunlight shining on photoactive regions of the electrode produces electric current to drive the hydrogen and oxygen evolution reactions (HER, OER) at opposite surfaces. In the conceptual design for a large-scale reactor shown in Fig. 2a, arrays of photoelectrodes are arranged in tubular reactors, and electrolyte

* Corresponding author.
E-mail address: ericm@hawaii.edu (E.L. Miller).

0360-3199/03/$ 30.00
PII: S0360-3199(02)00144-1

is circulated to extract the high-purity hydrogen and oxygen gases produced. As shown in Fig. 2b, the integrated photoelectrodes would be installed within membranes along the tubes which allow ion exchange, but not gas flow to effect hydrogen and oxygen separation.

In order to meet the DOE's goals, a PEC system must be low-cost, operate at solar-to-hydrogen (STH) conversion efficiencies greater than 10%, and have long operating lifetimes in the corrosive aqueous electrolyte environment. In accordance with Eq. (1) [2], the 10% STH efficiency corresponds to a hydrogen current density, J_T, of 8.1 mA/cm^2 at AM 1.5:

$$\underbrace{\eta_{STH}(\%)}_{\substack{\text{solar-to-hydrogen}\\ \text{efficiency}}} = \frac{1.23 J_T}{E_T} \times 100 = 1.23 \underbrace{J_T}_{\text{mA/cm}^2}$$

$$\text{for } \underbrace{E_T = 100 \text{ mW/cm}^2}_{\text{AM 1.5}}. \quad (1)$$

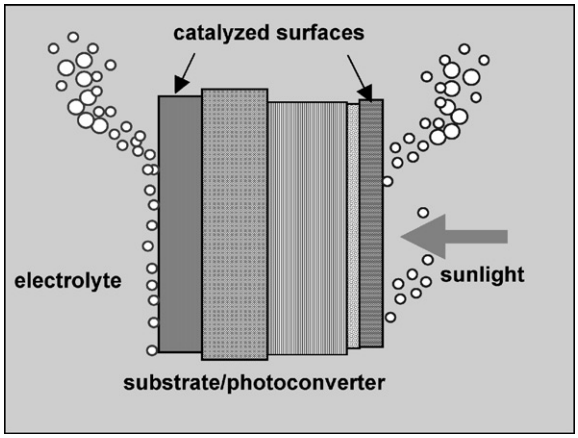

Fig. 1. Photoelectrochemical hydrogen production using an integrated planar photoelectrode.

Numerous approaches involving a variety of semiconductors have been explored for hydrogen photoelectrolysis since the early 1980s, but none have successfully satisfied both the efficiency and stability criteria. The high voltage required to dissociate water (the 1.23 V dissociation potential, plus additional voltage drops associated with overpotential and system losses) and the corrosiveness of aqueous electrolytes have been major hurdles in this effort.

Based on results from numerous modeling and proof-of-concept experiments conducted at UH over the course of its PEC research, an approach has been to developed to design photoelectrode configurations incorporating multijunction thin-film photoconvertors (for high voltage) along with thin-film catalyst and protective layers (for stability). A recent advance in the research has been the design of a "hybrid" photoelectrode structure combining solid-state junctions with photocatalyst semiconductor films that can form a stable rectifying photoelectrochemical junction at the electrolyte interface. This paper describes the design approach for developing efficient integrated photoelectrode configurations, with an emphasis on the design of the hybrid device for hydrogen production.

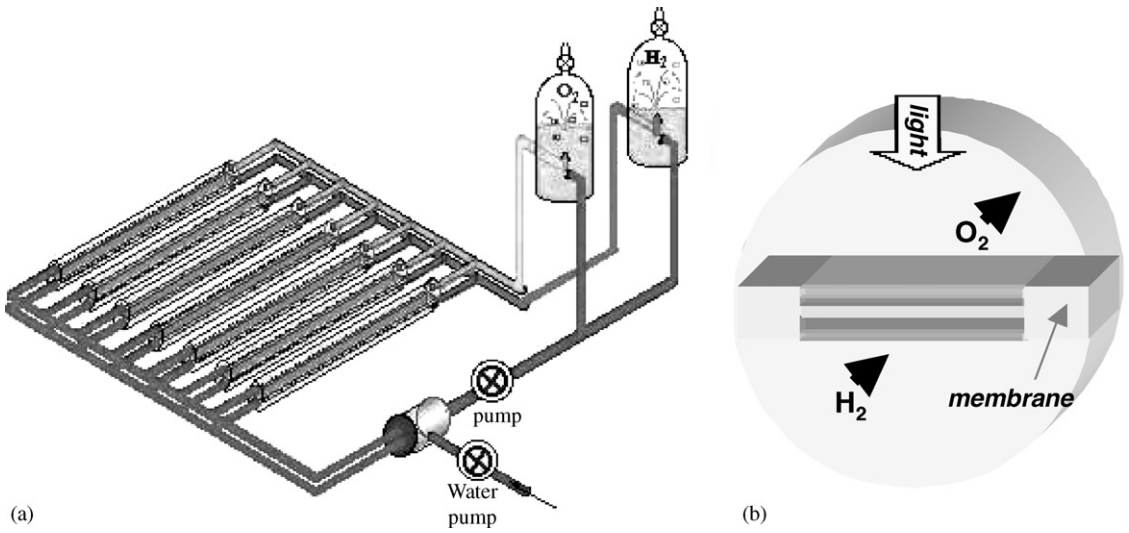

Fig. 2. (a) Conceptual design of large-scale reactor with integrated photoelectrodes; (b) photoelectrode installation in collection tubes with membrane for gas separation.

2. Integrated photoelectrode evolution

Research at UH to design integrated photoelectrodes for directly splitting water into hydrogen and oxygen has evolved through several stages. This evolution is traced in Fig. 3. As shown in Fig. 3a, the original configuration used single-crystal, p-type silicon with an OER catalyst layer on the back surface, and scattered islets of platinum HER catalyst deposited onto the front (light-entering) surface. Here the semiconductor/electrolyte junction formed the photovoltaic diode, and the HER islets facilitated current exchange. In the second stage photoelectrode, shown in Fig. 3b, the front surface was evenly coated with Shottky-barrier metal, followed by HER catalyst layers thin enough for optical transmission, effectively replacing the semiconductor/liquid junction with a rectifying semiconductor/metal junction. The first two designs were fabricated using planar processing exclusively and were fully integrated on a single substrate. While these did result in a net energy savings, the voltage generated was below that required to split water, necessitating external biasing. Corrosion resistance was also poor.

The third-generation photoelectrode shown in Fig. 3c incorporated several breakthrough features: First, the single-junction crystalline silicon diode was replaced by a triple-junction amorphous silicon diode (a pinpinpin device deposited onto a glass/CTO substrate in this configuration). Second, HER and OER thin-film catalysts of sputter-deposited NiMo and Fe:NiOx [3,4], respectively, developed at UH specifically for low overpotentials and for long life in KOH, were used. A small prototype based on this configuration achieved solar-to-hydrogen efficiencies up to 7.8% [1]. Since only catalyst surfaces were exposed to the electrolyte, excellent corrosion resistance was also achieved. The primary disadvantages were the use of separated electrodes and the need for external wiring.

The external wiring was eliminated in the fourth-generation photoelectrode shown in Fig. 3d. A stainless-steel substrate was coated on the front side with a triple nipnipnip junction amorphous silicon/germanium (a-Si:Ge)diode and thin ITO and OER catalyst films, and on the back side with HER catalyst. The disadvantage was that light entered through the OER catalyst, leading to additional optical loss. With the metal oxide catalyst developed to date, films thin enough for good optical transmission offered little corrosion protection to underlying films, necessitating highly corrosion-resistant ITO and amorphous silicon. The fourth-generation photoelectrodes were fully integrated onto a single substrate and were fabricated using all planar processing techniques; however, the prototypes constructed all suffered from reduced efficiency due to the optical losses and from poor stability in KOH due to the thin protective/catalyst layer.

An important new feature in the fifth-generation photoelectrode structure pictured in Fig. 3e is the incorporation of a highly transparent and corrosion-resistant encapsulation film that does not need to be conductive. As in the previous configuration, the HER catalyst is sputter-deposited onto the back of a stainless-steel substrate, and a-Si:Ge nipnipnip and ITO layers are deposited onto the front. Next, OER catalyst is sputter-deposited through a shadow mask onto a specified fraction of the diode's surface, and the encapsulation film is deposited through a second mask onto the remaining fraction to form a protected window for transmitting light. Light enters through the encapsulated window while current is transported through the catalyst surface; this precludes the need for ultra-thin/transparent OER catalyst films. High efficiency requires modest concentration to focus the light onto the window region. This design is fully integrated onto a single substrate using a sequence of straightforward planar processing steps. A significant advantage is that only high-stability surfaces are exposed directly to electrolyte. Disadvantages include the added component of lateral current collection, added fabrication complexity at the front surface, and front-surface seams (e.g., catalyst and encapsulated window edges) that could result in device degradation over long exposure to electrolyte.

Another major advantage in the fifth-generation integrated photoelectrode with encapsulation is in the opportunity it affords for stacking the series-connected multijunction solid-state cells side-by-side as well as monolithically. As a result, higher-efficiency materials such as copper–indium–gallium–diselenide (CIGS), which cannot stack monolithically, can be used as an alternative to a-Si:Ge. Figs. 4a and b show, respectively, the basic design structures for multijunction encapsulated photoelectrodes with monolithically stacked a-Si:Ge and with side-by-side stacked CIGS.

Both Fig. 4 device structures, in particular the CIGS device in Fig. 4b, represent a significant increase in fabrication complexity over previous generation photoelectrodes. In both, lateral collection of current through the ITO represents an efficiency-reducing loss. The reduced surface area of the front surface catalyst also degrades hydrogen conversion performance. Despite the disadvantages, enhanced stability through encapsulation of underlying semiconductor layers is an attractive feature. Also of importance, both the a-Si:Ge and CIGS photoelectrode systems have the potential for low cost based on the very thin semiconductor layers involved and on compatibility with high-throughput manufacturing processes.

As discussed in the device modeling section below, even with the additional current-collection and catalyst area-reduction losses, model results indicate solar-to-hydrogen efficiencies in excess of 10% for the CIGS photoelectrode; unfortunately, predicted efficiencies drop below 10% for the encapsulated a-Si:Ge structure. This is explained in part by the higher photovoltaic efficiency in CIGS, which can approach 19% [5], compared with a-Si:Ge, which has to date demonstrated peak efficiencies up to only 13% [6]. Another factor is the comparative losses associated with the reduced front surface catalyst

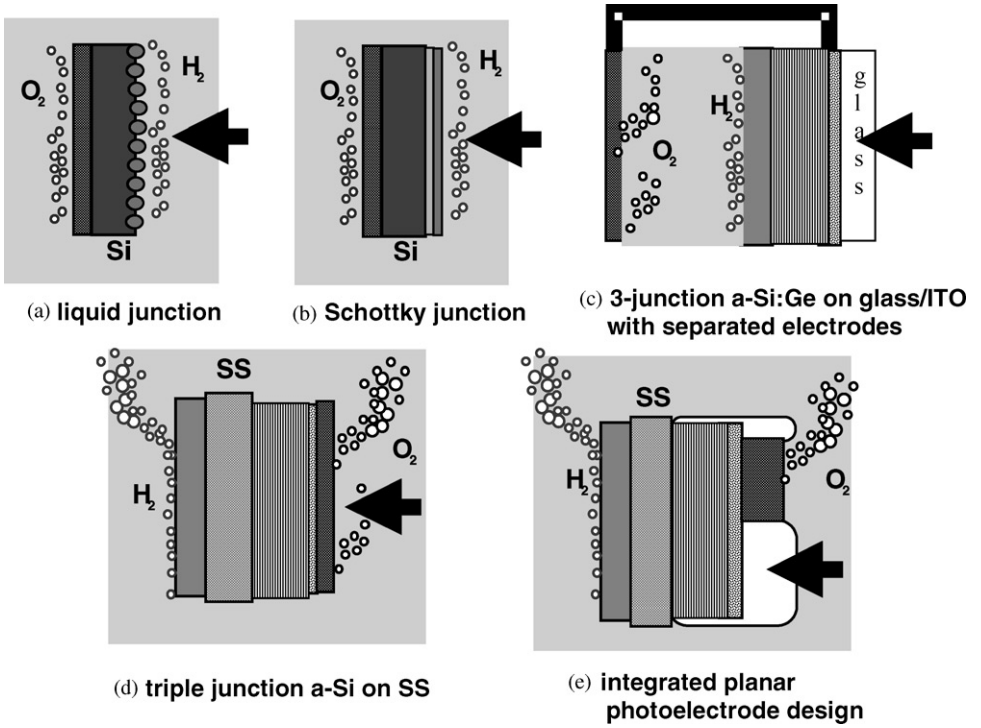

Fig. 3. Evolution at UH of planar photoelectrodes for solar-to-hydrogen conversion.

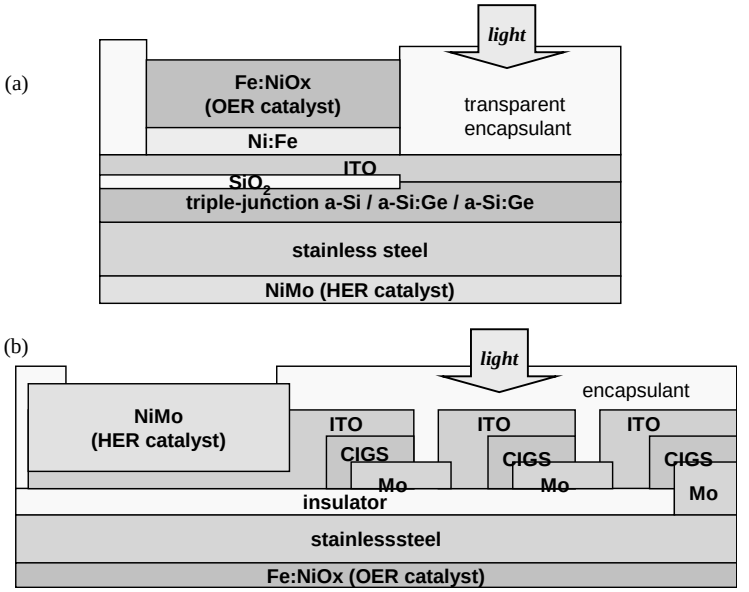

Fig. 4. Structure of encapsulated triple-junction photoelectrode using (a) a-Si:Ge ; (b) CIGS.

areas in the two configurations. For optimal PV efficiency in a-Si:Ge cells, light should enter through the p-layer, dictating OER catalyst on the front surface. In CIGS cells, where light enters through the n-layer, the front surface must be catalyzed for the HER. Since HER overpotentials are generally lower than those for the OER with available catalysts, reduced HER front-surface catalyst in the CIGS cells represents a less severe loss.

3. Integrated photoelectrode modeling

Analyzing the operation of hydrogen photoelectrodes requires a complex integration of photovoltaic, optical, and electrochemical phenomena, and an important part of the UH research has been the development of integrated models combining these effects [7,8]. The elements of these models, based on a lumped-circuit model of a photocell in series with a current-dependent electrochemical load, are shown in Fig. 5a for a triple-junction photocell. In this analysis, the dark diode characteristics are estimated from the performance of high-quality devices reported in the literature. The light *JV* characteristics of the photocells are calculated assuming superposition with light-generated currents and complete absorption of photons with energies above the optical gap and complete transmission of those below it. The electrochemical model (shown in the right-hand side of Fig. 5a) uses the Butler–Volmer relation to describe the current-dependent overpotentials due to charge transfer kinetics at the electrode surfaces, and included additional resistances for the potential drop due to ion transport through the electrolyte. Kinetic parameters used in the model are based on values achieved in thin-film, sputter-deposited catalysts developed at UH [3,4], and the decomposition potential (V_{eq}), along with system resistances (R_{ec}), are taken from the literature.

Outputs from this integrated analysis include the current–voltage (*JV*) curve of the photocell and the load curve of the electrochemical cell. The intersection of these two curves defines the operating point of the system, as illustrated in the load-line analysis plot in Fig. 5b. For the various semiconductor systems investigated—thin film amorphous silicon/germanium, Group III–V crystalline cells, and thin film CIGS—different combinations of bandgaps and electrochemical parameters were examined to identify designs with the highest expected hydrogen production rates. Even with highly optimistic assumptions for the diode characteristics (i.e., small reverse saturation currents), the analysis showed that semiconductor bandgaps greater than 1.9 eV are required to generate voltages sufficient for direct water-splitting when single-junction photoelectrodes are considered. The analysis also showed that any loss in junction or catalyst performance in such single-photon systems would result in large performance losses, requiring even higher bandgaps to provide a reasonable probability of stable operation. The poor absorption of the solar spectrum with such high bandgaps results in low quantum efficiency and poor photovoltaic/photoelectrochemical performance.

Of the materials evaluated in multijunction photoelectrodes, those based on crystalline Group III–V heterojunctions showed the highest theoretical solar-to-hydrogen (STH) conversion efficiencies, with values as high as 20% in tandem structures. The high cost of these materials, however, makes them impractical for commercial PEC systems. Because of their good voltage match, STH conversion efficiencies for the much lower-cost multijunction a-Si:Ge structures were predicted to be as high as 10%. Moreover, it was predicted that STH efficiencies approaching 15% are possible using the encapsulated photoelectrode designs with multijunction copper–indium–gallium–diselenide (CIGS) cells stacked in a side-by-side configuration [9]. Of significance, both the a-Si:Ge and CIGS-based photoelectrodes can be fabricated on low-cost substrates such as metal foils. They have further potential for low cost based on the very thin semiconductor layers involved and on compatibility with high-throughput manufacturing processes.

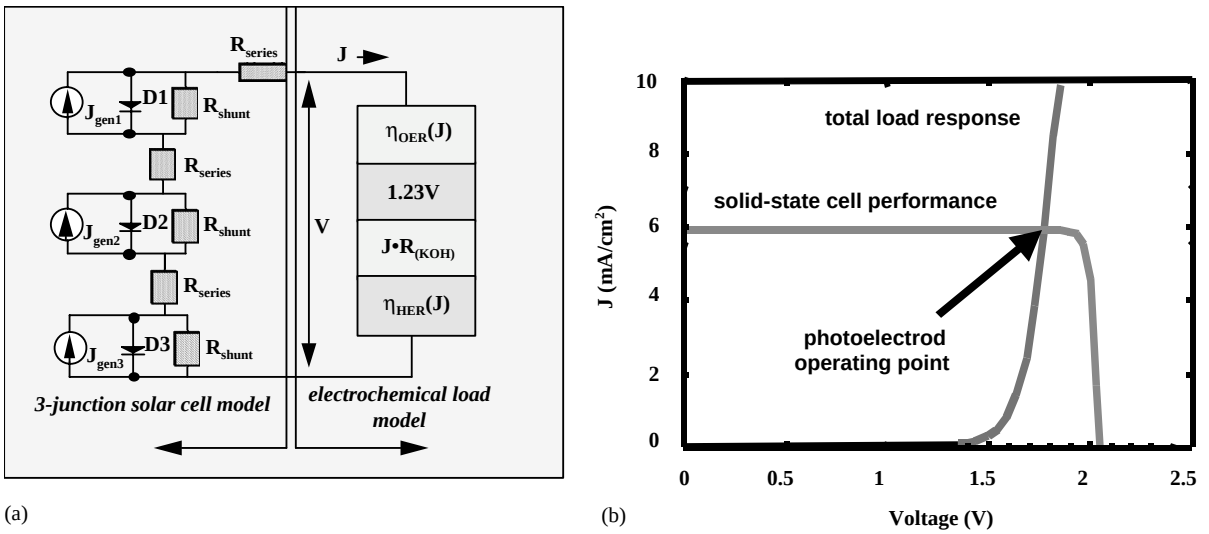

Fig. 5. (a) Model of triple-junction photoelectrode; (b) load-line analysis to determine photoelectrochemical operating point.

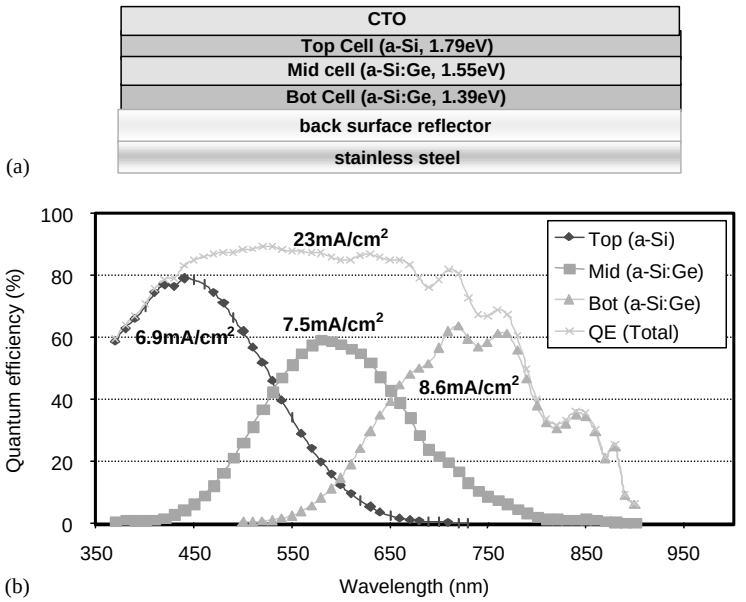

Fig. 6. (a) Structure of the Toledo 12.7% triple-junction a-Si/a-Si:Ge/a-Si:Ge solar cell; (b) AM 1.5 quantum efficiencies and integrated currents for component cells and multijunction device.

4. Hybrid photoelectrodes

As an alternative approach to both the integrated a-Si:Ge and CIGS photoelectrode structures, which utilize photogeneration in multiple connected solid-state junctions, UH recently developed a conceptual design for a hybrid solid-state/PEC photoelectrode incorporating current-matched solid-state and electrochemical photojunctions. This design was in part motivated by recent advances in semiconductor materials, such as dye-sensitized TiO_2, WO_3, and Fe_2O_3, for photoelectrochemical applications. The design process was greatly facilitated by use of the integrated modeling approach for photovoltaic and photoelectrochemical systems . For example, triple junction a-Si:Ge solar cells demonstrating photovoltaic efficiencies up to 12.7% and open-circuit voltages up to 2.3 V have recently been deposited onto stainless-steel foil substrates by the University of Toledo [6]. The fundamental design strategy for producing such high efficiency in multijunction amorphous silicon/germanium devices involved careful current matching in each of the junctions by adjustment of the absorption spectra through bandgap and i-layer thickness tailoring. The basic device structure, shown in Fig. 6a, incorporates three component nip cells, with i-layer bandgaps ranging from 1.79 to 1.55 to 1.39 eV in the top, middle, and bottom cells, respectively. The top layer conductive-transparent oxide (CTO) is used to collect front-surface current, while the back surface reflector layer is used to reflect back photons and boost quantum efficiency (QE). Fig. 6b shows the QE curves for this device, along with the AM 1.5 integrated currents for the component cells, and for the total combined device. Since device current will be limited by the lowest-current cell in the series-connected stack, current-matching in the component cells is critical for good performance. In current-matching, the total device integrated current should be equally divided into each of the component cells to fully utilize the total photogenerated carriers.

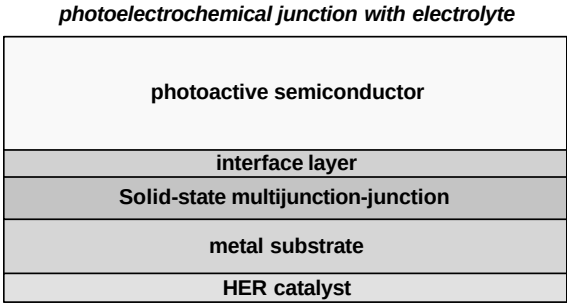

Fig. 7. Basic structure for a hybrid solid-state/photoelectrochemical photoelectrode.

As seen Fig. 6b, the top nip junction in the 12.7% device is designed to absorb most strongly in the 350–500 nm range. In principle, this top cell could be replaced or amended by a PEC junction with strong absorption in a similar range to form a water-splitting photoelectrode for hydrogen production. As shown in Fig. 7, this hybrid photoelectrode can be fabricated on stainless-steel foil with the back surface catalyzed for the HER. Deposited onto the front surface are a

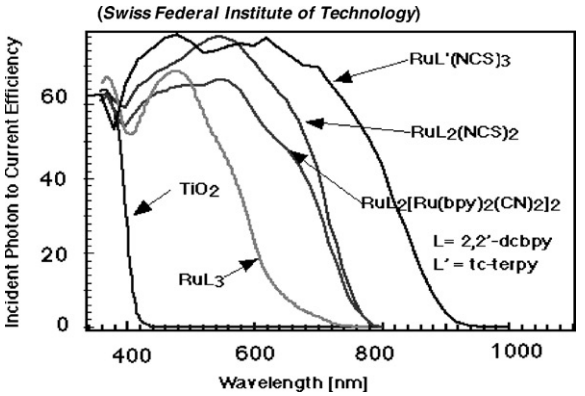

Fig. 8. Quantum efficiencies in dye-sensitized TiO_2 photoelectrochemical junctions.

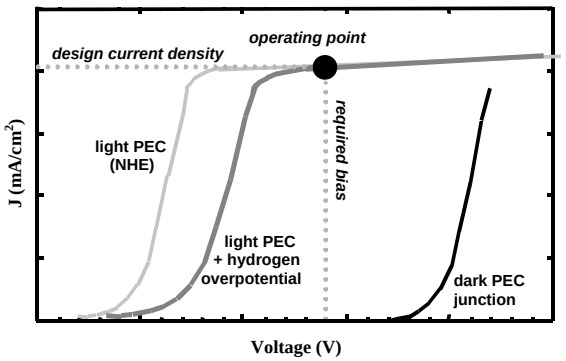

Fig. 9. Load-line analysis of the hybrid photoelectrode configuration.

solid-state multijunction followed by a CTO interface layer, then by a photoactive-semiconductor layer (i.e., a photocatalyst). The semiconductor top layer, which forms a PEC junction in electrolyte, must have appropriate conduction band alignment for the OER, must be strongly absorbing in the 350–500 nm region for current-matching to the underlying solid-state junctions, and must be stable. Significant advantages of the hybrid design over the encapsulated design from Fig. 3e include elimination of the lateral current collection, reduction in OER overpotential, enhanced stability due to the thick uniform photocatalyst layer (typically several microns), and greatly simplified geometry for ease of fabrication.

Research advancements in dye-sensitized titanium dioxide (TiO_2), tungsten trioxide (WO_3), and iron oxide (Fe_2O_3) indicate that these may be suitable candidate materials for the hybrid photoelectrode. Fig. 8, for example, shows the quantum efficiencies (stated in IPCE or incident photon conversion efficiency) of TiO_2 PEC junctions as a function of sensitizing dye [10]. The junction sensitized with the RuL_3 dye exhibits peak absorption near 500 nm, consistent with the requirements for the hybrid photoelectrode. Interestingly, photoelectrochemical photovoltaic cells based on dye-sensitized TiO_2 have been successfully demonstrated using the I^-/I_3^- couple [11]. Unfortunately, however, inherent instability in all currently known dyes under OER conditions make this versatile material unsuitable for the hybrid hydrogen photoelectrode, at least at this time. Continued research into new dyes that remain stable under oxidation is reportedly underway [12].

Current literature concerning WO_3 [13] and Fe_2O_3 [14] indicate that forms of these wide-bandgap photocatalytic materials remain stable for the OER. To evaluate the potential use of these materials, a form of the previously described integrated load-line analysis can be used. The technique, which requires both the light *JV* and quantum efficiency characteristics of the photocatalyst interface, is illustrated in Fig. 9. The design operating current of the device is dictated by efficiency goals, as per Eq. (1). Referring to the curves in Fig. 9, the light *JV* response of the PEC junction with respect to the normal hydrogen electrode (NHE) must be corrected to account for the current-dependent hydrogen overpotential loss occurring at the back surface of the device. The intersection of this corrected curve with the design current gives the required bias to be supplied by the underlying solid-state multijunction. This solid-state device must be designed to generate the design current at the required bias using the photons not absorbed in the PEC junction. This is where knowledge of the PEC quantum efficiency becomes critical for an overall optical balance.

The model can be used to evaluate hybrid systems using, for example, nanostructured WO_3 as the photocatalyst. Fig. 10 shows the photocurrent response (Fig. 10a) and the quantum efficiency (Fig. 10b) of WO_3 nanostructured films prepared at the University of Geneva [13]. The HER overpotential correction to the light *JV* curve shown in Fig. 10a is based on performance of the UH-developed thin film catalysts. In this *JV* plot, the peak photocurrent of this junction occurs at approximately 2.5 mA/cm^2. This low current can be understood in terms of the WO_3 quantum efficiency curve in Fig. 10b, which peaks around 85%, but which spans only a narrow region in the blue wavelengths (a spectrum consistent with the nominal bandgap of 2.7 eV for tungsten trioxide). An important result from applying integrated modeling techniques is that the operating point of 2.5 mA/cm^2 at a voltage bias of 1.5 V is readily achievable with a properly designed a-Si:Ge double junction.

Also shown in Fig. 10b is the QE of the top cell of the Toledo 12.7% solid-state device. It is evident that replacing this top cell with a WO_3 junction to form a hybrid photoelectrode does not extend the useful collection range of the device. As a result, the peak total photocurrent available remains at about 24 or 8 mA/cm^2 for each of the three junctions (two solid-state and one PEC) in the hybrid device. Unfortunately, the peak PEC photocurrent represents a bottleneck, limiting device current in the hybrid structure to only 2.5 mA/cm^2 (a STH efficiency of 3.1%). Since the top

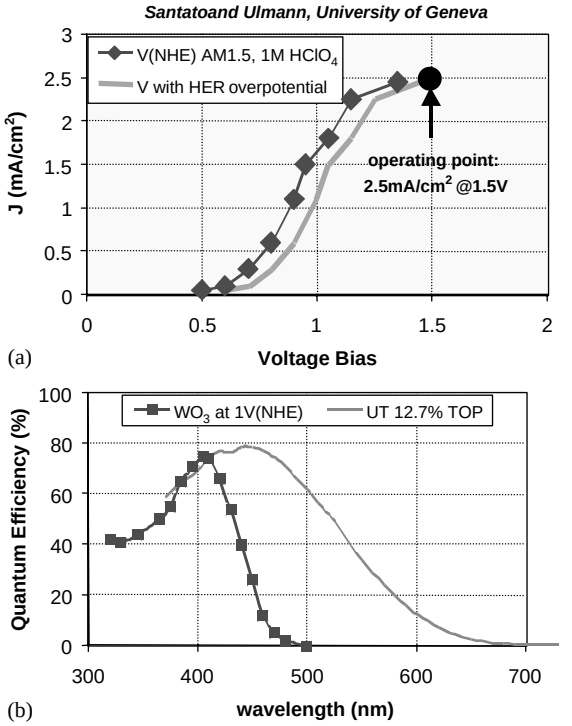

Fig. 10. (a) Photocurrent response; (b) quantum efficiency of nanostructured WO_3 films.

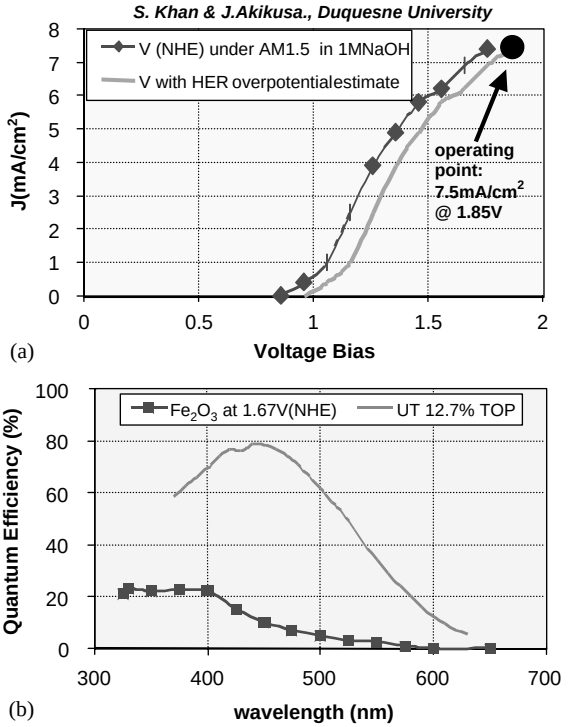

Fig. 12. (a) Photocurrent response; (b) QE of nanostructured Fe_2O_3 films.

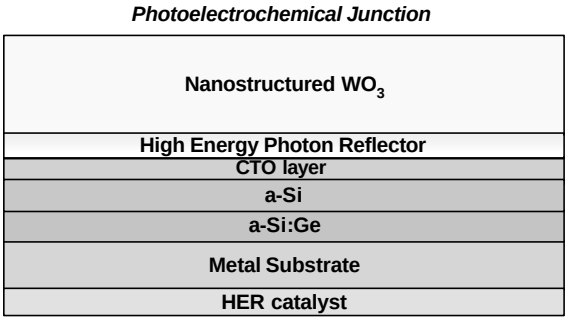

Fig. 11. Proposed structure for a tungsten trioxide hybrid photoelectrode.

PEC junction dictates performance, significant efficiency increases can be expected with material improvements in the WO_3 photocatalyst. In addition to the material improvements, creative techniques in the design of the hybrid structure can be used to boost efficiency. For example, in one possible configuration for a hybrid WO_3 photoelectrode, as shown in Fig. 11, an intermediate conductive layer beneath the tungsten trioxide could be designed with the correct refractive index and thickness to reflect high-energy photons back into the photocatalyst. The effective increase in optical path length can increase quantum efficiency in the WO_3, resulting in improved photocurrent and efficiency. Further investigation into this design technique is in progress.

Another candidate photocatalyst material for the hybrid structure, which is attractive based on recent published data, is iron oxide (Fe_2O_3). AM 1.5 photocurrent response based on data published by Khan and Akikusa at Duquesne University [14] for their nanostructured iron oxide films is shown in Fig. 12a, while quantum efficiency for these films is shown in Fig. 12b. In contrast to the tungsten trioxide photocatalyst, current densities near the 8.1 mA/cm^2 goal are readily achievable in the nanostructured iron oxide, as seen in Fig. 12a. Compared with WO_3, Fe_2O_3 has a relatively low bandgap of 2.1 eV, consistent with the observed spread in the quantum efficiency curve in Fig. 12b. Although the QE never exceeds 23%, integration of the AM 1.5 spectrum over a broad band of wavelengths accounts for the high levels of photogenerated current in the illuminated junction.

A performance limitation in the iron oxide hybrid photoelectrode is not a current bottleneck, but rather a relatively high-voltage bias constraint. For example, the operating point in Fig. 12a of 7.5 mA/cm^2 at 1.8 V could not be driven by a double junction a-Si/a-Si:Ge or a-Si:Ge/a-Si:Ge device according to modeling results. A triple-junction, solid-state cell would be required at this bias, resulting in

a quadruple-junction hybrid photoelectrode (one PEC and three solid-state junctions). Since total photocurrent needs to be split equally into four parts for current-matching, 10% STH conversion efficiency (8.1 mA/cm^2) would require a total integrated photocurrent of 32.4 mA/cm^2 in the combined solid-state/Fe_2O_3 junctions. With clever optical designs (e.g., back surface reflectors) and with the extended blue wavelength collection from the Fe_2O_3, this may be possible. However, as in the case of tungsten trioxide, significant improvements in the hybrid photoelectrode performance would result from nominal advances in iron oxide material properties. With a reduction in required voltage bias at 7.5 mA/cm^2 from 1.8 to 1.6 or 1.5 V, a double-junction, solid-state cell could be designed with good current-matching. Developing a hybrid device based on this abundant and low-cost material with solar-to-hydrogen conversion efficiencies exceeding 10% would then be a simple matter.

5. Conclusions

In this paper, we have described how integrated electronic/optical/electrochemical modeling is extremely useful in the development systems for photoelectrochemical hydrogen production. The modeling can be applied generally to PV systems and PV-driven electrolyzers, but at UH it is also be used to develop integrated photoelectrode systems in which planar solid-state multijunctions drive catalyzed areas on a single substrate, as well as integrated hybrid photoelectrode systems which combine solid-state and photoelectrochemical junctions to drive the water-splitting process. Significant results from the photoelectrode research effort at UH based on this modeling have included: demonstration of 7.8% solar-to-hydrogen efficiency in a triple-junction amorphous silicon/germanium photoelectrode deposited on glass/ITO with a separate anode; and an encapsulated integrated photoelectrode design based on a side-by-side stacked CIGS triple junction with potential STH conversion efficiency up to 15%.

Recent progress at UH in the development of hybrid photoelectrode designs utilizing stable, wide-bandgap semiconductor photocatalysts in conjunction with a-Si:Ge multijunctions is also encouraging. In particular, systems based on nanostructured tungsten trioxide or iron oxide appear promising. With continued improvements in photocatalyst materials properties, and with innovative design approaches, simple hybrid structures based on low-cost WO_3 or Fe_2O_3 with solar-to-hydrogen efficiencies exceeding 10% are expected. Quantum efficiency enhancement in tungsten trioxide and voltage bias reduction in iron oxide are of particular importance. An alternative, but also attractive, hybrid system based on dye-sensitized TiO_2 photocatalysts is contingent upon the success of sensitizing dyes that remain stable under oxidation.

Acknowledgements

We wish to thank the U.S. Department of Energy for support of this work under Grant DE-FG04-94AL85804. We also thank John Turner of the National Renewable Energy Laboratory and Clara Santato of the University of Geneva for their input concerning tungsten trioxide films. We wish to express special appreciation to the organizers of ICAM 2001.

References

[1] Rocheleau RE, Miller EL, Misra A. High-efficiency photoelectrochemical hydrogen production using multijunction amorphous silicon photoelectrodes. Energy Fuels 1998;12:3–10.
[2] Scaife DE. Oxide semiconductors in photoelectrochemical conversion of solar energy. Solar Energy 1980;25:41–54.
[3] Miller EL, Rocheleau RE. Electrochemical behavior of reactively sputtered iron-doped nickel oxide. J Electrochem Soc 1997;144(9):3072–7.
[4] Miller EL, Rocheleau RE. Electrochemical and electrochromic behavior of reactively sputtered nickel oxide. J Electrochem Soc 1997;144(6):1995–2003.
[5] Tuttle J. Thin-film $Cu(In,Ga)Se_2$ materials and devices: a versatile material for flat plate and concentrator photovoltaic applications. Soc Photo-Opt Instrum Engrs 1995;2531:194–200.
[6] Wang W, Liao XB, Han S, Povolny H, Xiang XB, Du W, Deng X. Triple-junction a-Si-based solar cells with all absorber layers deposited at the edge of a-Si to μc-Si transition, 2001, <http://www.physics.utoledo.edu/~dengx/ref3.pdf>.
[7] Rocheleau RE, Miller EL. Photoelectrochemical production of hydrogen: engineering loss analysis. Int J Hydrogen Energy 1997;22(8):771–82.
[8] Rocheleau RE, Vierthaler M. Optimization of multijunction a-Si:H solar cells using an integrated optical/electrical model. In: Proceedings of the 21st World Conference on Photovoltaic Energy Conversion, Honolulu, Hawaii, Institute for Electrical and Electronics Engineers, 1994. p. 567–70.
[9] Miller EL, Rocheleau RE. Photoelectrochemical hydrogen production. In: Proceedings of the 2000 U.S. Department of Energy Hydrogen Program Annual Review Meeting, San Ramon, California, U.S. Department of Energy, 2000.
[10] Graetzel M. The artificial leaf, bio-mimetic photocatalysis. Catech 1999;3(1):4–16.
[11] Swiss Federal Institute of Technology. Dye-sensitized solar cells based on nanocrystalline oxide semiconductor films, 1996, <http://dcwww.efl.ch/icp/ICP-2/solarcellE.html>.
[12] Konigstein C. Some aspects of photochemical systems for direct light-induced hydrogen production. J Photochem Photobiol A 1995;90:141–52.
[13] Santato C, Ulmann M, Augustynski J. Photoelectrochemical properties of nanostructured tungsten trioxide films. J Phys Chem B 2001;105:936–40.
[14] Khan SUM, Akikusa J. Photoelectrochemical splitting of water at nanocrystalline n-Fe_2O_3 thin-film electrodes. J Phys Chem B 1999;103:7184–9.